



Degree Project in Technology

First cycle, 15 credits

# **Demonstrating quantum entanglement and the Hong-Ou-Mandel effect**

Using type-II spontaneous parametric down conversion with C programming for data collection.

**JOHAN JOHANNISSON LUNDQUIST & ERIK SVANBERG**

## **Acknowledgement**

We would like to thank our supervisor Marcin Swillo who helped us throughout the project.

## **Abstract**

Spontaneous parametric down conversion (SPDC) is used to generate quantum entangled photons through a non-linear crystal. The entanglement of photons is demonstrated by observing the effects of indistinguishability on photons, first through time and energy, then by polarization. The Hong-Ou-Mandel (HOM) effect was also demonstrated. A theoretical derivation of the effect of a non 50/50 beam splitter (BS) is also investigated. The energy of the photons was changed by varying the temperature of the crystal whilst the time difference was changed by varying the relative position of two mirrors. Results showed a clear effect from indistinguishability on both energy and time.

## **Sammanfattning**

Spontaneous parametric down conversion används för att generera kvantsammanflätna fotoner genom en icke-linjär kristall. Denna sammanflätning är sedan påvisad genom att observera effekten av icke-särskiljbarhet av fotoner, först genom tid och energi, sedan genom polarisation. Hong-Ou-Mandel effekten har även påvisats. En teoretiskt härledning av effekten från en icke 50/50 stråldelare är också undersökt. Energin av fotoner ändrades genom att variera temperaturen av kristallen medans tidsskillnaden ändrades genom att variera den relativa positionen av två speglar. Resultaten visade en tydlig effekt från icke-särskiljbarhet på både energi och tid.

# Contents

<b>List of abbreviations</b>	<b>4</b>
<b>1 Introduction</b>	<b>5</b>
<b>2 Theoretical background</b>	<b>5</b>
2.1 Spontaneous Parametric Down Conversion . . . . .	5
2.2 Hong-Ou-Mandel effect . . . . .	6
2.3 Impact on Hong-Ou-Mandel effect from non 50/50 beam splitter	8
2.4 Ensuring indistinguishability . . . . .	10
<b>3 Experimental Setup</b>	<b>12</b>
3.1 Spontaneous parametric down conversion . . . . .	13
3.2 Testing indistinguishability . . . . .	13
3.3 Hong-Ou-Mandel effect . . . . .	14
3.4 Registering photons . . . . .	15
<b>4 Data collection with Raspberry Pi</b>	<b>17</b>
4.1 Program functionality . . . . .	17
4.2 Program usage . . . . .	17
4.3 Effectiveness of program . . . . .	18
<b>5 Results</b>	<b>18</b>
5.1 Indistinguishability . . . . .	18
5.2 HOM . . . . .	19
<b>6 Discussion</b>	<b>21</b>
6.1 Comparison of results . . . . .	21
6.2 Improving the indistinguishability . . . . .	22
<b>7 Conclusion</b>	<b>22</b>

## List of abbreviations

SPDC - Spontaneous parametric Down Conversion  
ppKTP - periodically poled Potassium Titanyl Phosphate  
HOM - Hong-Ou-Mandel  
PBS - Polarising beam splitter  
BS - Beam splitter  
QWP - Quarter-Wave plate  
HWP - Half-Wave Plate  
SPD - Single photon detector  
H - Horizontal  
V - Vertical  
A - Anti-diagonal  
D - Diagonal  
o - ordinary  
e - extraordinary  
i - idler  
s - signal  
p - pump

# 1 Introduction

Quantum entanglement is a non-classical effect that generated great mystery and discussion between physicists when it was first discovered. Nowadays there exists a great deal of theory behind this phenomenon. However, the real life consequences are much more difficult to fathom. This paper studies how one can create quantum entangled photons and to observe the Hong-Ou-Mandel effect (HOM). It also discusses how indistinguishability is an important concept for quantum entangled particles.

However, creating indistinguishable photons can be quite difficult. They need to be indistinguishable in time, wavelength and polarization. Imperfect optical tools, such as misaligned optical components or non 50/50 beam splitters, can also negatively impact results.

## 2 Theoretical background

This section describes the theoretical background to the experiments that are described later on. Firstly, the method of generating quantum entangled photons through type-II Spontaneous Parametric Down Conversion (SPDC) is explained. The section is then followed by a description of the Hong-Ou-Mandel (HOM) effect [4]. It is then concluded with discussions regarding the impact of the quality of beam splitters (BS) and the importance of ensuring indistinguishability of the photons.

### 2.1 Spontaneous Parametric Down Conversion

SPDC is a way of generating quantum entangled photons using a non-linear crystal. In this experiment a periodically poled Potassium Titanyl Phosphate crystal (ppKTP) will be used which generates quantum entangled photons of different polarization, i.e type-II SPDC. In type-II SPDC, a pump (p) photon enters a non-linear crystal which then splits it into two photons of orthogonal polarization (ordinary and extraordinary, denoted with index o and e respectively) known as signal (s) and idler (i) [3].

The Hamiltonian for the SPDC can be derived from the expression of potential field energy  $U_E = \epsilon_0 \int_V \mathbf{E} \cdot \mathbf{P} dV$  where  $\mathbf{P}$  is the polarization and  $\mathbf{E}$  is the electric field. This is however omitted from this report and for derivation see [1]. The Hamiltonian then becomes:

$$\hat{H}_{SPDC} = i\hbar\kappa(\hat{a}_i^\dagger \hat{a}_s^\dagger \hat{a}_p e^{-i\Delta\mathbf{k}\cdot\mathbf{r}+i\Delta\omega t} + h.c) \quad (1)$$

where  $\Delta\mathbf{k} = \mathbf{k}_p - \mathbf{k}_s - \mathbf{k}_i$  and  $\Delta\omega = \omega_p - \omega_s - \omega_i$ . Additionally,  $\hat{a}$  and  $\hat{a}^\dagger$  stands for the destruction and creation operator respectively, and indices s, i and p stand for signal, idler and pump. Furthermore,  $\kappa$  is a constant and h.c. stands for the hermitian conjugate.

Consider now this Hamiltonian applied to the state  $|0_s, 0_i, N_p\rangle$ , which represents  $N$  pump photons entering the crystal. Using the Schrödinger equation,

$\hat{H} |\psi(t)\rangle = i\hbar \frac{\partial}{\partial t} |\psi(t)\rangle$ , the state then becomes

$$|\psi(t)\rangle = e^{\frac{1}{i\hbar} \int_0^t \hat{H}_{SPDC}(t') dt'} |0_s, 0_i, N_p\rangle. \quad (2)$$

Note that  $\kappa$  in equation (1) is small. Thus a first order Taylor expansion can be used, resulting in the following expression:

$$|\psi(t)\rangle \approx C_0 |0_s, 0_i, N_p\rangle + C_1 \frac{1}{i\hbar} \int_0^t \hat{H}_{SPDC}(t') dt' |0_s, 0_i, N_p\rangle \quad (3)$$

where  $C_0$  and  $C_1$  come from normalization requirements. Note that  $\hat{a}_i^\dagger \hat{a}_s^\dagger \hat{a}_p$  applied to the state  $|0_s, 0_i, N_p\rangle$  creates  $|1_s, 1_i, N_p - 1\rangle$ . Also that  $\hat{a}_i |0_i\rangle = 0$  and therefore the h.c part from equation (1) disappears. Thus equation (3) becomes:

$$|\psi(t)\rangle = C_0 |0_s, 0_i, N_p\rangle + C_1 \kappa e^{-i\Delta\mathbf{k}\cdot\mathbf{r}} \frac{e^{i\Delta\omega t} - 1}{i\Delta\omega} |1_s, 1_i, N_p - 1\rangle \quad (4)$$

Perfect energy conservation between photons gives  $\hbar\omega_p = \hbar(\omega_i + \omega_s)$ . Assuming close to perfect energy conservation then gives  $\Delta\omega \approx 0$ . This means that  $\frac{e^{i\Delta\omega t} - 1}{i\Delta\omega} \approx 1$  and equation (4) becomes:

$$|\psi(t)\rangle = C_0 |0_s, 0_i, N_p\rangle + C_1 \kappa e^{-i\Delta\mathbf{k}\cdot\mathbf{r}} |1_s, 1_i, N_p - 1\rangle \quad (5)$$

It is important to note that  $C_0 \gg C_1$  and thus SPDC does not happen for most photons. However, for those that it does, the resulting state is the signal-idler pair with orthogonal polarization.

## 2.2 Hong-Ou-Mandel effect

The HOM effect can be seen when measuring the joint detection probability ( $p_c$ ) of two detectors registering a photon pair, which can be generated in a process such as SPDC described above. By letting the pair interfere on a 50/50 BS and varying the difference in optical path length one can observe a sharp decline in  $p_c$ . Alternatively, a similar dip can be seen by varying the crystal temperature in the photon-pair generation setup. This phenomenon is called the HOM dip [3].

This effect can be derived from theory, but that is outside the scope of this thesis. For a rigorous derivation see [1], who arrives at the following expression for  $p_c$ :

$$p_c = 1/2(1 - \rho(\omega_d, \tau)) \quad (6)$$

where

$$\rho(\omega_d, \tau) = \begin{cases} (\omega_d \tau_0)^{-1} \sin(\omega_d \tau_0 [1 - \tau_0^{-1}(\tau - \tau_0)]) , & 0 \leq \tau < DL \\ 0 , & \text{otherwise.} \end{cases} \quad (7)$$

The variable  $\tau$  denotes the time delay between s and i photon pair, while  $\omega_d = \frac{1}{2}(\Omega_o - \Omega_e)$  signifies the detuning of the two, where  $\Omega_o$  and  $\Omega_e$  are the frequencies

of o and e polarizations. The upper-bound  $DL$  of  $\tau$  for a non-zero  $\rho(\omega_d, \tau)$  originates from the fact that s and i are generated simultaneously inside the crystal, travelling at different speeds inside, resulting in a limit to the maximum time delay. Lastly,  $\tau_0$  is defined as  $\tau_0 \equiv DL/2$ , which is the time delay resulting in the wave packets coinciding, i.e. the complete erasure of distinguishability with regards to time. With  $\tau = \tau_0$ , equation (7) gets reduced to:

$$\rho(\omega_d, \tau = \tau_0) = \text{sinc}(\omega_d \tau_0) \quad (8)$$

Which has been utilized in combination with equation (6) to plot  $p_c$  in figure 1 below.

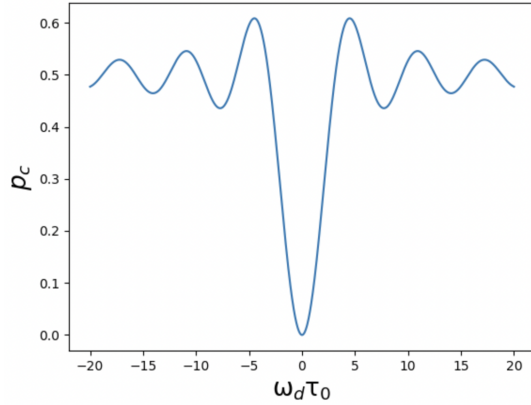


Figure 1: Plot of the joint detection probability  $p_c$  with equation (6) and (8), with the non-dimensionalized argument  $\omega_d \tau_0$ .

Similarly if  $\omega_d = 0$ , i.e both photons have the same frequency and therefore wavelength, equation (7) becomes:

$$\rho(\omega_d = 0, \tau) = \begin{cases} 1 - \tau_0^{-1}(\tau - \tau_0) , & 0 \leq \tau < DL \\ 0 , & \text{otherwise.} \end{cases} \quad (9)$$

Equation (9) together with (6) is used to plot  $p_c$  below in figure 2.

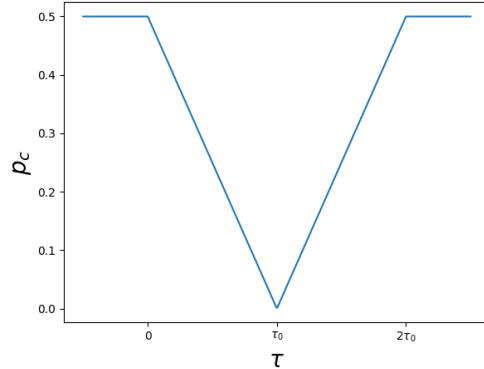


Figure 2: Plot of the joint detection probability  $p_c$  versus  $\tau$  with  $\omega_d = 0$ .

Figure 2 shows a clear triangular shape which is characteristic for the HOM dip in time. This comes from the overlapping of rectangular wave functions where at  $\tau = \tau_0$  the wave functions completely overlap causing the probability to become zero.

### 2.3 Impact on Hong-Ou-Mandel effect from non 50/50 beam splitter

Above in section 2.2 the BS has been assumed to be perfectly 50/50. However, in reality it can be quite difficult to align it as such and some BS have defects. The question then becomes how the strength of the HOM effect or rather the depth of the dip changes with an imperfect BS. Figure 3 shows how photons enter at port A and B and exit at port C and D of a BS.

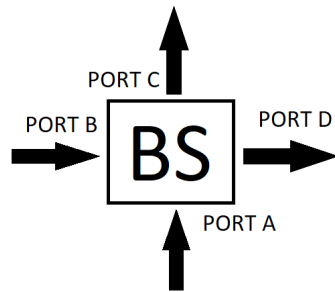


Figure 3: Visualisation of the BS. Photons enter in port A and B and exit at port C and D.

Two inputs  $I_a$  and  $I_b$  enter at port A and B whilst two outputs  $O_c$  and  $O_d$  exit at port C and D respectively. If  $R$  and  $T$  are the reflection and transmission

coefficients then  $I_a \rightarrow TO_c + RO_d$  and  $I_b \rightarrow RO_c + TO_d$ . Then the matrix representation becomes:

$$\begin{pmatrix} I_a \\ I_b \end{pmatrix} = \begin{pmatrix} T & R \\ R & T \end{pmatrix} \begin{pmatrix} O_c \\ O_d \end{pmatrix} = B \begin{pmatrix} O_c \\ O_d \end{pmatrix}$$

In the BS matrix, B, elements can be determined by assuming a lossless BS. For a lossless BS the matrix must be unitary since the norm of the input and output must remain the same. Thus  $BB^\dagger = BB^{-1} = I$ . This gives:

$$\begin{pmatrix} T & R \\ R & T \end{pmatrix} \begin{pmatrix} T^* & R^* \\ R^* & T^* \end{pmatrix} = \begin{pmatrix} 1 & 0 \\ 0 & 1 \end{pmatrix}$$

Hence the equations become:

$$|T|^2 + |R|^2 = 1, \quad RT^* + R^*T = 0. \quad (10)$$

Since transmission and reflection coefficients are complex numbers they can be written as  $T = |T|e^{i\theta_1}$  and  $R = |R|e^{i\theta_2}$ . The angles  $\theta_1$  and  $\theta_2$  are both relative phases and thus  $\theta_1$  can be set to zero. Consequently, equation (10) gives:

$$|R||T|e^{i\theta_2} + |R||T|e^{-i\theta_2} = 2|R||T|\cos\theta_2 = 0 \Rightarrow \theta_2 = \pi/2. \quad (11)$$

Now set  $|T| = x$  and equation (10) then gives  $|R| = \sqrt{1-x^2}$ . The BS matrix now becomes:

$$B = \begin{pmatrix} x & i\sqrt{1-x^2} \\ i\sqrt{1-x^2} & x \end{pmatrix}. \quad (12)$$

Now consider a photon entering port A,  $|1\rangle_A = a^\dagger |0\rangle_A$ . Together with the matrix B the state will then become:

$$a^\dagger |0\rangle_A = x|1\rangle_C + i\sqrt{1-x^2}|1\rangle_D = xc^\dagger |0\rangle_C + i\sqrt{1-x^2}d^\dagger |0\rangle_D. \quad (13)$$

Similarly for a photon entering the B port:

$$b^\dagger |0\rangle_B = i\sqrt{1-x^2}|1\rangle_C + x|1\rangle_D = i\sqrt{1-x^2}c^\dagger |0\rangle_C + xd^\dagger |0\rangle_D. \quad (14)$$

The operator  $a^\dagger$  and  $b^\dagger$  are thus:

$$a^\dagger = xc^\dagger + i\sqrt{1-x^2}d^\dagger, b^\dagger = i\sqrt{1-x^2}c^\dagger + xd^\dagger. \quad (15)$$

Now if two indistinguishable photons, in both time, frequency and polarization, enter the BS the state before is  $|1_A, 1_B, 0_C, 0_D\rangle$ . Hence with equation (15) the state becomes:

$$\begin{aligned} |1_A, 1_B, 0_C, 0_D\rangle &= a^\dagger b^\dagger |0_A, 0_B, 0_C, 0_D\rangle = \{(15)\} = \\ &= (xc^\dagger + i\sqrt{1-x^2}d^\dagger)(i\sqrt{1-x^2}c^\dagger + xd^\dagger) |0_A, 0_B, 0_C, 0_D\rangle = \\ &= (ix\sqrt{1-x^2}(c^\dagger)^2 + ix\sqrt{1-x^2}(d^\dagger)^2 + x^2c^\dagger d^\dagger - (1-x^2)d^\dagger c^\dagger) |0_A, 0_B, 0_C, 0_D\rangle = \\ &= \{(a^\dagger |n\rangle = \sqrt{n+1}|n+1\rangle)\} = \\ &= ix\sqrt{1-x^2}\sqrt{2}(|0_A, 0_B, 2_C, 0_D\rangle + |0_A, 0_B, 0_C, 2_D\rangle) + (2x^2 - 1)|0_A, 0_B, 1_C, 1_D\rangle \\ &= \xi_{2,0}|0_A, 0_B, 2_C, 0_D\rangle + \xi_{0,2}|0_A, 0_B, 0_C, 2_D\rangle + \xi_{1,1}|0_A, 0_B, 1_C, 1_D\rangle. \end{aligned}$$

The probability  $p_{i,j} = |\xi_{i,j}|^2$  for each corresponding state. Therefore the quantum probabilities become:

$$p_{2,0,quantum} = p_{0,2,quantum} = 2x^2(1-x^2), \quad p_{1,1,quantum} = (2x^2 - 1)^2 \quad (16)$$

Where  $p_{i,j}$  corresponds to the probability that  $i$  photons exit port C and  $j$  photons exit port D. However, in order to examine how this affects the HOM effect one also needs to consider the probabilities if they are completely distinguishable particles. This calculation can be done classically by considering one photon entering at a time. Using the coefficients in equation (13) and (14) the probabilities become:

$$p_{2,0,classic} = p_{0,2,classic} = x^2(1-x^2), \\ p_{1,1,classic} = x^4 + (1-x^2)^2 = 2x^4 - 2x^2 + 1 \quad (17)$$

Since the depth of the HOM dip is based upon the probability that one photon exits each port and is always relative to the distinguishable case the percentual relative size at the bottom will become:

This gives the normalized coincidence probability (i.e., the probability of detecting one photon in each output port, relative to the classical case).

$$\frac{p_{1,1,quantum}}{p_{1,1,classic}} = \frac{4x^4 - 4x^2 + 1}{2x^4 - 2x^2 + 1} \quad (18)$$

Using equation (16), (17) and (18) with different transmission probabilities,  $x^2$ , some examples of probabilities are shown in table 1.

$x^2$	$p_{1,1,classic}$	$p_{1,1,quantum}$	Depth of dip
0	1.0	1.0	1.0
0.1	0.82	0.64	0.78
0.3	0.58	0.16	0.28
0.5	0.5	0	0

Table 1: Probabilities for two distinguishable and indistinguishable exiting two different ports in a BS depending on transmission probability  $x^2$ . Depth of dip is the relative probability between the indistinguishable and distinguishable case.

The expected results are shown in table 1. When the transmission probability is zero there is no dip whatsoever and when the probability is  $1/2$  the dip goes to 0. Note that the probability functions are symmetric around  $x^2 = 0.5$  and thus it does not matter if the probability is skewed in favor of reflection or transmission. Given that the transmission probability are known for a particular BS, equation (18) thus gives the value of the deepest possible HOM dip.

## 2.4 Ensuring indistinguishability

In order to fully ensure indistinguishability of photons a second test needs to be devised. In this test a similar effect will be observed in order to ensure indistinguishability in time and frequency.

The state,  $|H, V\rangle$ , generated from type-II SPDC enters a BS. If they are indistinguishable, this will turn the state into  $\frac{1}{2}(|V\rangle_A|H\rangle_B + |V\rangle_B|H\rangle_A + |V\rangle_A|H\rangle_A + |V\rangle_B|H\rangle_B)$ : where A and B reference the two different exit ports of the BS, while V and H denotes vertical and horizontal polarisation respectively. This is shown in figure 4 below.

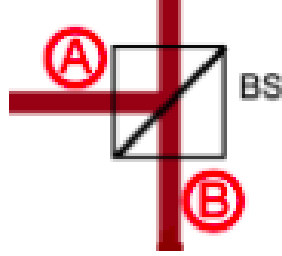


Figure 4: Visualisation of the first BS. Photons exit at A and B.

The only parts that will provide coincidences to be measured are the ones where both photons leaves each port:

$$\frac{1}{\sqrt{2}}(|V\rangle_A|H\rangle_B + |V\rangle_B|H\rangle_A) \quad (19)$$

where  $\frac{1}{\sqrt{2}}$  comes from normalisation. This is a polarization entangled state, which can be used to test indistinguishability in different bases. Photons generated with H and V polarization will be used, where the latter will be converted to the former for the demonstration of the HOM effect. Therefore, it is of interest to test the diagonal (D) and anti-diagonal (A) polarization:

$$|D\rangle = \frac{1}{\sqrt{2}}(|V\rangle + |H\rangle), |A\rangle = \frac{1}{\sqrt{2}}(|V\rangle - |H\rangle). \quad (20)$$

Figure 5 shows a visualisation of A and D polarization.

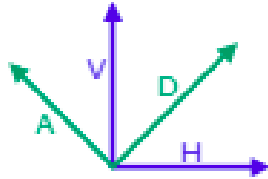


Figure 5: Visualisation of A and D polarization compared to V and H.

Using equation (20), the states  $|H\rangle$  and  $|V\rangle$  can be rewritten as:

$$|V\rangle = \frac{1}{\sqrt{2}}(|D\rangle + |A\rangle), |H\rangle = \frac{1}{\sqrt{2}}(|D\rangle - |A\rangle). \quad (21)$$

Hence equation (21) into equation (19) gives:

$$\frac{1}{\sqrt{2}}(|V\rangle_A|H\rangle_B + |H\rangle_A|V\rangle_B) = \frac{1}{\sqrt{2}}(|D\rangle_A|D\rangle_B - |A\rangle_A|A\rangle_B) \quad (22)$$

This means that the state is a superposition of both photons being diagonal and antidiagonal. By then putting a polarizer with  $45^\circ$  after the A port and a polarizer with  $-45^\circ$  after the B port (or vice versa) the photons cannot pass both polarizers. This is because the  $45^\circ$  polarizer would block A but allow D to pass, whilst the  $-45^\circ$  polarizer would block D but allow A. Thus, if both photons are indistinguishable in both time and energy, the joint detection probability will go to zero, confirming polarization entanglement of the photon-pair.

### 3 Experimental Setup

The experimental setup can be divided into two parts. The first part consists of the non-linear crystal together with alignment tools and a compensator for the temporal delay that occurs when the two photons travel at different speeds through the crystal and the lenses. The second part consists of beam splitters which can be used, with slight variations in the setup, to test indistinguishability using A and D polarized photons as well as the HOM effect.

An image of the real life setup is shown in figure 6. The detailed description of the parts are explained in the subsections below.

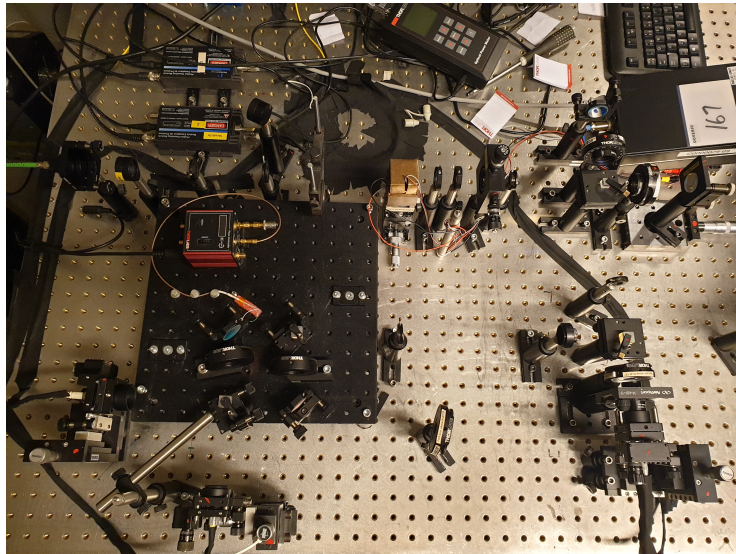


Figure 6: Image of the lab setup.

### 3.1 Spontaneous parametric down conversion

Here follows an explanation of the setup used for creating quantum entangled photons through SPDC and compensation of the temporal delay. A visualisation of the setup is shown below in figure 7.

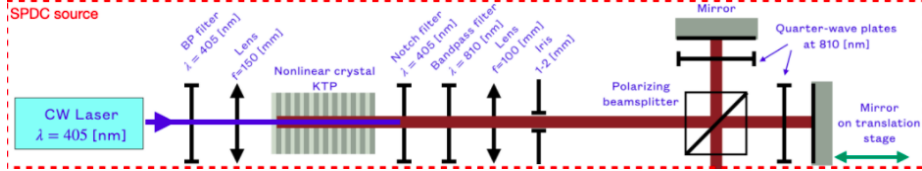


Figure 7: Visualisation of the setup for SPDC and compensation of temporal delay. Image from [2].

The pump photons are provided from a laser with wavelength  $\lambda_p = 405\text{nm}$ . First a bandpass filter (BP) is used to only transmit the pump photons with  $405\text{nm}$  wavelength and other light sources coming from the optic fiber in the laser are removed. Then there is a lens focusing the beam onto the non-linear ppKTP crystal. Inside the crystal SPDC occurs, resulting in two-photon generation. Directly after the crystal a notch filter stops all light with wavelength  $405\text{nm}$ , followed by a BP that transmits only light with wavelength  $\lambda = 810\text{nm}$ .

As the s and i photons are generated, they exit the crystal at an angle. Thus, they diverge. In order for them to go parallel to each other, a lens is used. Finally, an iris is utilised to only allow photons that are close to each other to pass through. If the photons have diverged a lot they are far from each other and therefore more distinguishable.

Due to the different refractive indices inside the crystal, as well as the difference in path length that comes from the later part of the experiment, the photons do not travel next to each other. Therefore, in order to adjust this temporal delay, a polarizing beam splitter (PBS) is used to split the photons. A PBS allows H photons to pass but reflects V photons at a  $90^\circ$  angle. The photons travel through a quarter-wave plate (QWP) that rotates the polarization  $45^\circ$  into circular polarized light. These are then reflected in a mirror travelling back through the QWP causing both photons to have their polarization rotated  $90^\circ$  in total. H photons pass through the PBS and after rotation are vertical, causing them to be reflected when entering the second time. The opposite happens for the V photons. For the H photons the distance to the mirror can be adjusted in order to compensate the temporal delay.

### 3.2 Testing indistinguishability

To make sure a reliable result is gathered when doing measurements for the HOM effect, the indistinguishability of the photons need to be confirmed. To test the indistinguishability, the setup shown in 8 below was used in combination

with the SPDC setup. This is similar to the Bell test for a polarization entangled state[6].

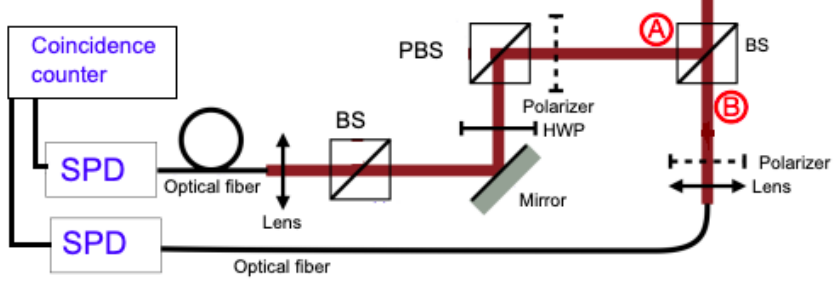


Figure 8: Visualisation of the setup used to ensure the indistinguishability of photons.

The first BS creates the entangled state shown in equation (22). The two polarizers ensure the dip in joint detection probability by one of the polarizers being set to  $45^\circ$  whilst the other is  $-45^\circ$ .

The PBS will split the A or D polarized photon 50/50 whilst the HWP will change its polarization. However, this has no relevance. The PBS, HWP and BS after the A port are only there to be used for different experiments.

Lastly, the photons travel through optical fibers to reach single photon detectors (SPD). These converts the photons to an electrical signal that is then passed to a TDC1 coincidence counter.

The optical path difference, as well as the frequency of the photons, are changed in order to ensure indistinguishability. By gradually changing the optical path difference, a dip in coincidence measurements will be observed when the photons become more and more indistinguishable in time.

### 3.3 Hong-Ou-Mandel effect

The setup used for the HOM effect is shown below in figure 9.

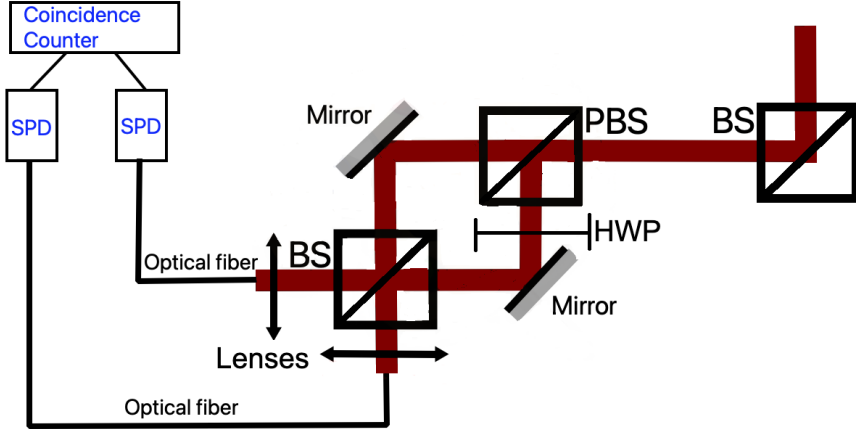


Figure 9: Visualisation of the setup used to create the HOM effect.

First the photons enter a BS. This is not necessary for the HOM effect, however, as this setup is also used for testing indistinguishability as mentioned previously it is kept there for ease of use.

Secondly the two photons enter a PBS. Here H photons pass through and V photon are reflected 90°. The H and V photons are then both reflected onto a mirror and the V photons pass through a half-wave plate (HWP) that rotates the polarization 90° to make the V photons H.

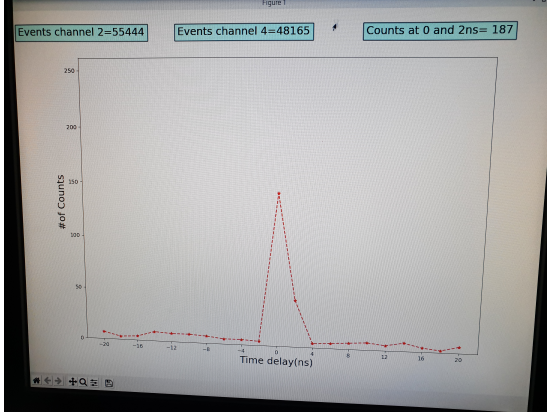
Since the photons are now indistinguishable in polarization, if they are also indistinguishable in time and frequency, the HOM effect will be observed upon exiting the final BS. As such the two photons cannot exit different ports of the BS and both must leave through the same port. Thus the counter should not see any coincidences and the HOM dip is observed.

To study the HOM effect, two types of measurements were made. As discussed in section 2.2, the joint detection probability  $p_c$  depend on the time delay  $\tau$  of the s and i photon pair and the detuning  $\omega_d$ . The effects of the former can be measured by incrementally varying the optical path length of one of the paths and noting the coincidence rate at each point. In practice, this is done by adjusting the translation position of the mirror in figure 7. The latter can similarly be studied by incrementally changing the temperature of the crystal, which separately affects the refractive indices  $n_o$  and  $n_e$ . Thus, the frequencies of the two polarizations alter, resulting in variations in  $\omega_d$ .

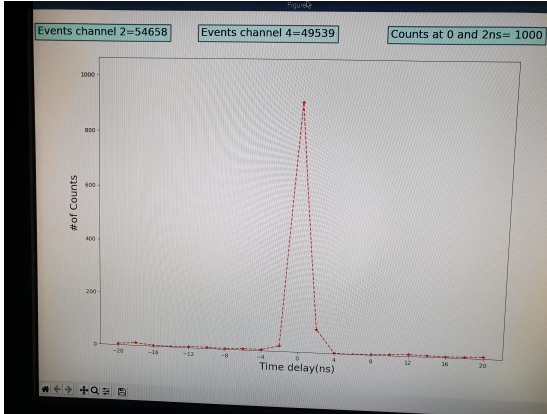
### 3.4 Registering photons

The coincidence counter is a TDC1 time to digital converter that register at what time and which port an electrical signal entered. Since there can be a time difference from the different lengths of the optical cables the computer program will show a histogram that counts coincidences that happen at a certain time

difference. For example if two electrical signals entered in different channels with 4 ns time difference this will add 1 count to 4 ns. Two examples of this graph is shown below in figure 10.



(a) Image from the program when photons were close to indistinguishable.



(b) Image from the program with distinguishable photons.

Figure 10: Two images of the program used when plotting coincidences. The first graph is when the photons are close to indistinguishable whilst the second is when the photons are distinguishable. Note that the y-axis is rescaled and the amount of coincidences can be seen in the upper right corner.

As figure 10 shows, the graphs have similar total events in both channels. However, figure 10a has much lower amount of coincidences. This is due to the HOM effect.

## 4 Data collection with Raspberry Pi

This section explains how the program for the data collection is implemented and how to use it. The purpose of this is to allow other people to do these experiments using the same equipment and program. The full program and code can be found on GitHub [8]. The effectiveness of the program is also discussed as the speed of the program is of importance and thus the calculations were implemented in C.

### 4.1 Program functionality

The program works as follows: The python file, plot\_timestamp.py, is responsible for plotting the results and calls the C part of the program. The C part, timestamp\_calculation.c, is responsible for establishing connection with the coincidence counter via USB and does the calculations for the histogram.

The python program uses ctypes in order to call the C program. Matplotlib is used for plotting and by turning on interactive mode allows the graph to be continuously updated as new data is collected.

The C program opens the serial port and initializes the device. The initialization is based upon a tutorial [5] and settings are taken from the TDC1 documentation [7]. The TDC1 box sends 32-bit events which is split into 4 bytes. The first 27 bits correspond to the time at which the event happened and the last 5 bits correspond to which channel detected an event.

The programs then compares two following events in order to determine if they happened in different channels and if they had less than a 20 ns time difference between them. If it did happen within 20 ns the time difference is then added to a histogram in which each position in the histogram corresponds to a 2 ns time interval.

As such, the time difference that arises from the length difference of the cables can be accounted for. When the laser is then turned on there will be a clear peak at a certain time difference, which comes from the length difference of the cables.

### 4.2 Program usage

In order to use the program only the python part needs to be called. The python part later calls the C part via:

```
lib = cdll.LoadLibrary("/home/pi/lab/timestamp_measurement/calc.so")
```

Note that the location is correct for the Raspberry Pi which the program was used on, but will need to be changed on other computers. The program will automatically register which port the USB counter is in. If not an exception will be thrown. Parts of the program can be easily changed if required. The time that the program collects information can be changed with the following line:

```
t_collect = 1.0 #Collect data for 1 second
```

Note that the plot will take slightly longer to update since it takes time to plot. The time that it collects for will also be longer than the given time since the elapsed time is only checked at the beginning of the while loop in the C code:

```
while( elapsed < t_collect ){
```

Therefore the time that it collects for should not be chosen too short. Furthermore, there are two options that can be chosen in the code.

```
str3 = "Counts_at_" + ... + str(histo[time_pos]+histo[time_pos2])
str3 = "Maximum_counts_at_" + ... + str(histo[time_pos])
```

The first option will show the total amount of coincidences at the two times that have the largest amount of coincidences. The second only shows the largest amount of coincidences at the corresponding time. The former option is mostly used. The reason for this is because the TDC1 has a resolution of 2 ns. Hence, if the time difference is somewhere in-between an even number, such as 3 ns, then the peak will be spread out between 2 and 4 ns in the histogram.

It is important to note that the C program is multi-threaded to utilise the 4 cores in Raspberry Pi. Therefore, the program splits the input into 4 arrays, thus increasing the calculation speed. Using the program on a single core unit will cause it to be slower.

Lastly if one needs to change the C program, the following compile command should be used:

```
cc -fPIC -shared -fopenmp -o calc.so timestamp_calculation.c
```

### 4.3 Effectiveness of program

Initially, there was a similar program written in Python for the data collection. However, this program was too slow in order to show any good result with HOM effect. The laser was only used at an effect of 2-3 mW. With the new program the laser has been used for effects as high as 30 mW. Higher effects than this has not been tested. The program can at best compute slightly lower than 1 million events per second. This was tested by connecting the TDC1 to a function generator.

## 5 Results

This section presents the results from the two setups. First for the test of indistinguishability and then for the HOM effect.

### 5.1 Indistinguishability

In figure 11 below the results for the indistinguishability measurements is shown. For each point, an average of 5 consecutive values were taken, collected continuously during 1 second for each value.

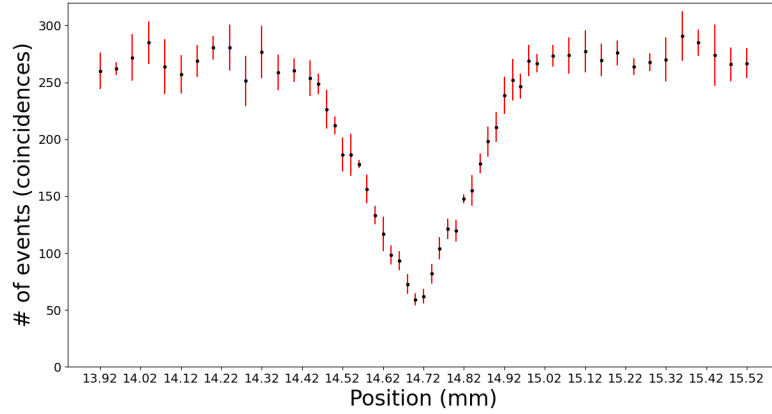


Figure 11: Plot of coincidence rates versus position, showing a dip in the amount of coincidences. Each value was taken as an average over 5 points and error bars are shown in red. The temperature was set to  $19.0^{\circ}C$ . The lowest point is at 14.70 mm.

Figure 11 shows HOM dip when the mirror is positioned at 14.70 mm. This is when photons are most indistinguishable and enter the first BS simultaneously. As the photons enter with larger time difference their wave functions overlap less and less, causing more coincidences to happen. At around 0.5 mm away from the lowest part of the dip the photons becomes completely distinguishable.

## 5.2 HOM

The HOM dip in both temperature and position are shown below in figure 12 and figure 13 respectively. Similarly to the last experiment, every single measured point was taken as an average of 5 values and for each value photons were collected for 1 second.

Firstly the correct position and temperature had to be found roughly since when varying one variable the other had to be correct. Otherwise no dip could be observed. The position of the mirror was set to 13.16 mm. The temperature dip was calculated by incrementally changing the temperature  $0.2^{\circ}C$  at a time and observing coincidences at that temperature.

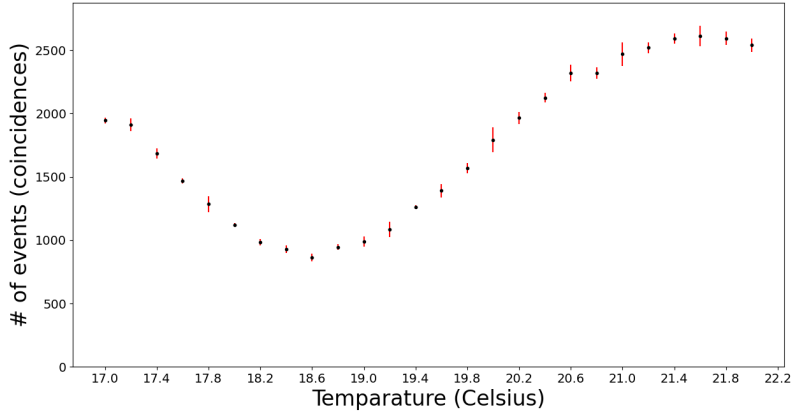


Figure 12: Coincidence rates versus temperature showing the HOM dip. Each value was taken as an average over 5 points and error bars are shown in red. The position was set to 13.16 mm. The lowest point is at  $18.6^{\circ}\text{C}$ .

The reason for the temperature measurements not going below  $17^{\circ}\text{C}$  or above  $22^{\circ}\text{C}$  is a consequence of the room temperature in the lab making it difficult to keep the crystal at temperatures above or below these values.

The lowest point in the temperature graph, figure 12, was at  $18.6^{\circ}\text{C}$ . This temperature was later used for the position measurement seen in figure 13 below.

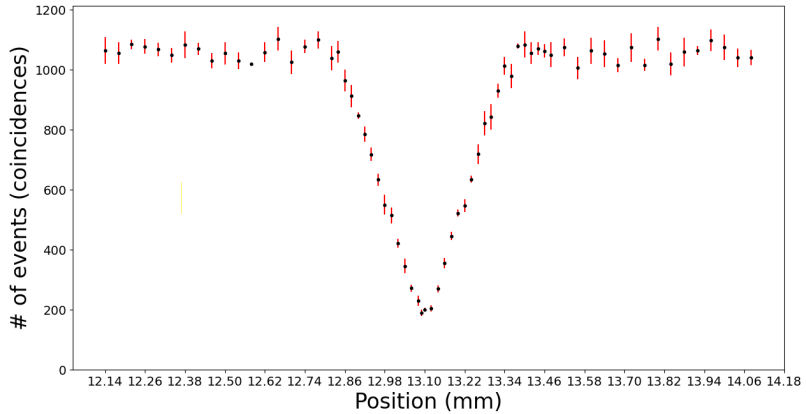


Figure 13: Coincidence rates versus position showing the HOM dip. Each value was taken as an average over 5 points and error bars are shown in red. The temperature was set to  $18.6^{\circ}\text{C}$ . The lowest point is at 13.09 mm.

As seen by comparing figure 12 and 13, the dip in total was much deeper in the position graph compared to the temperature graph. In the temperature graph the lowest value was roughly 33% that of the highest values. Whilst in the position graph the lowest value was almost 17% that of the higher values.

Note that the reason behind the difference in the dip position of figure 11 and figure 13 is due to the differences of optical path length needed in order to make the photons enter simultaneously at the BS. In figure 11 the photons converged at the first BS at 14.70 mm path difference, whilst in figure 13 the photons converged at the second BS at 13.09 mm path difference.

## 6 Discussion

Discussion will cover sources of errors and aims to investigate how the indistinguishability of photons can be increased for a deeper HOM dip. A comparison of the theoretical and experimental results will also be carried out.

### 6.1 Comparison of results

Comparing the graph from the experiment, figure 13, for the position HOM dip against the theoretical graph, figure 2, some similarities and differences are observed. The experiment showed the expected triangle shape from the theory. However, the probability (coincidences) did not go to zero. This is partly because the photons were not completely indistinguishable and also because the BS is believed to not be exactly 50/50. How much the distinguishability affected the results versus how much the BS did is not known. However, their combined effect produced a result that only reached 17% coincidence rate at the lowest compared to the distinguishable case.

The temperature graph from the experiment, figure 12, was also compared to the theoretical frequency graph, figure 1. The temperature graph vaguely resembles the expected results, but due to the incompleteness in the span of the temperature measurements it is hard to draw further conclusions. As the dip is quite shallow, this indicates a higher proportion of distinguishable photons.

This distinguishability comes partly from the imperfect positioning of the mirror, but also due to the size of the iris. As mentioned in section 3.1, the iris was used in order to remove photons that have diverged too far apart. After the temperature measurements the iris was adjusted, resulting in fewer distinguishable photons passing through.

For the position graph there might be an distinguishability in the frequency coming from the non-ideal temperature. This is due to the problems of keeping the temperature exact since it might change slightly during the course of the experiment. Another problem is that the temperature is not measured on the crystal, but instead a copper plate next to it. The thermal conductivity of the crystal is not known. Hence the temperature displayed is not necessarily the actual temperature of the crystal. The temperature controller also has an accuracy of  $\pm 0.1^\circ C$ .

## 6.2 Improving the indistinguishability

The main ways to improve indistinguishability is more precise temperature controls, position differences and better alignment. However, in order to measure this, perfect components are also necessary. As discussed in section 2.3, imperfect optical instruments in the setup can produce a non-zero dip despite photons being indistinguishable. There are also problems with detectors. Ambient light from the room enters the detector and causes coincidences randomly, despite photons being indistinguishable. There are also dark counts, i.e. photon detection without incident light, that also pose problems. Therefore it is impossible to reach the theoretical zero detection rate. However, much lower dips have been reached. For example, Florian Wolfgramm et al.[9], where values less than 5% of the distinguishable rates were achieved.

## 7 Conclusion

Firstly, the indistinguishability of photons in time and frequency was proven in the diagonal and anti-diagonal basis. This was done by testing the polarization entangled state.

Later this was followed up by measurements of the HOM effect using both temperature (frequency) and position (time). By noticing the clear dip in coincidences for both temperature and position the indistinguishability was shown in time, energy and polarization.

The dip did not reach the theoretical value of 0. Many reasons contribute to this such as imperfect optical equipment, non-optimal alignment, imprecision in measurements of temperature, photons from ambient light and to a small degree dark counts. The latter of these are the reason why it is impossible to reach zero coincidences with our current technology.

Nonetheless, by showing the indistinguishability of photons the quantum entanglement of these particles was also demonstrated.

## References

- [1] Ömer Bayraktar et al. “Quantum-polarization state tomography”. In: *Phys. Rev. A* 94 (2 Aug. 2016), p. 020105. DOI: 10.1103/PhysRevA.94.020105. URL: <https://link.aps.org/doi/10.1103/PhysRevA.94.020105>.
- [2] Gunnar Björk and Marcin Swillo. *Lab PM Quantum Erasure for Quantum Technology, SK2903*. November 2021.
- [3] Christophe Couteau. “Spontaneous parametric down-conversion”. In: *Contemporary Physics* 59.3 (2018), pp. 291–304.
- [4] Chong-Ki Hong, Zhe-Yu Ou, and Leonard Mandel. “Measurement of subpicosecond time intervals between two photons by interference”. In: *Physical review letters* 59.18 (1987), p. 2044.
- [5] Geoffrey Hunter. *Linux Serial Ports Using C/C++*. 2017. URL: <https://blog.mbedded.ninja/programming/operating-systems/linux/linux-serial-ports-using-c-cpp/> (visited on 03/22/2020).
- [6] Kurt Jung. “Polarization Correlation of Entangled Photons Derived Without Using Non-local Interactions”. In: *Frontiers in Physics* 8 (2020). ISSN: 2296-424X. DOI: 10.3389/fphy.2020.00170. URL: <https://www.frontiersin.org/article/10.3389/fphy.2020.00170>.
- [7] sifteen. *TDC1 Documentation*. Oct. 2019. URL: [https://github.com/s-fifteen-instruments/Timestamp\\_TDC1/wiki/TDC1-Documentation](https://github.com/s-fifteen-instruments/Timestamp_TDC1/wiki/TDC1-Documentation) (visited on 04/21/2022).
- [8] Erik Svanberg. *Timestamp data collection for TDC1 in C*. Version 1.0.0. Apr. 2022. URL: <https://github.com/Berget-Svanis/Timestamp-data-collection-for-TDC1-in-C/tree/main> (visited on 04/21/2022).
- [9] Florian Wolfgramm et al. “Bright filter-free source of indistinguishable photon pairs”. In: *Optics express* 16 (Nov. 2008), pp. 18145–51. DOI: 10.1364/OE.16.018145.

